ELSEVIER

Chemical Engineering Journal 140 (2008) 341–351

Chemical Engineering Journal

www.elsevier.com/locate/cej

Selection of appropriate fuel processor for biogas-fuelled SOFC system

P. Piroonlerkgul [a], S. Assabumrungrat [a,*], N. Laosiripojana [b], A.A. Adesina [c]

[a] *Center of Excellence in Catalysis and Catalytic Reaction Engineering, Department of Chemical Engineering, Faculty of Engineering, Chulalongkorn University, Bangkok 10330, Thailand*

[b] *The Joint Graduate School of Energy and Environment, King Mongkut's University of Technology Thonburi, Bangkok 10140, Thailand*

[c] *Reactor Engineering & Technology Group, School of Chemical Sciences & Engineering, University of New South Wales, Sydney, NSW 2052, Australia*

Received 9 August 2007; received in revised form 4 October 2007; accepted 5 October 2007

Abstract

The performance of biogas-fed solid oxide fuel cell (SOFC) systems utilizing different reforming agents (steam, air and combined air/steam) has been investigated via thermodynamic analysis to determine the most suitable feed. The boundary of carbon formation was first calculated to specify the minimum amount of each reforming agent necessary to avoid carbon formation. The SOFC performance (electrical efficiency and power density) was determined at different biogas compositions and reforming agent:biogas ratios. The SOFC performance is better when the methane content in the biogas is higher. Steam is considered to be the most suitable reforming agent in this study as the steam-fed SOFC offers much higher power density than the air-fed SOFC although its electrical efficiency is slightly lower. When steam is added in the air-fed SOFC as in the case of the co-fed SOFC, the power density can be improved but the electrical efficiency becomes lower compared with the case of the air-fed SOFC. Finally, in order to improve the electrical efficiency of the steam-fed SOFC, the biogas split option was proposed. It was found that a higher electrical efficiency can be achieved. In addition, although the power density is lowered by this operation, the value is still higher than the case of the air-fed SOFC.

Keywords: Biogas; Dry reforming; Partial oxidation; Solid oxide fuel cell; Steam reforming; Thermodynamic analysis

1. Introduction

The demand for fossil fuel in electrical power generation has significantly increased in the past decade due to the rapid changes in global economic activities. This upsurge in fossil fuel consumption poses serious fuel supply insecurity and increases the amount of greenhouse gases accumulating in the environment. To alleviate these problems, several environmental-friendly fuels have been proposed alternatives to conventional fossil fuels. Biogas is an attractive fuel as it is derived renewably from biomass and it contains only trace amount of non-methane hydrocarbons. A common problem for biogas utilization is that most biogas is derived from small-scale sources, e.g. farm and municipal wastes. Hence, the use of biogas is applicable to a small-size power generation (5–100 kW) [1]. Moreover, the biogas composition fluctuates markedly, depending on its source [2]. Generally, biogas contains methane (40–65%), carbon dioxide (30–40%) and trace of nitrogen.

A solid oxide fuel cell (SOFC) is an appropriate technology for generating electricity from biogas due to its high efficiency (30–40%) for small-size power generations (<20 kW) [1]. Recently, a 100 kW class SOFC system fed by biogas has been proposed, and the electrical efficiency of almost 48.7% [3] was reported compared to 41.5% of a conventional system [4]. Additionally, its performance is still remarkable even at low methane contents in biogas. In laboratory test, the performance of SOFC drops only 5% when the biogas composition (CH_4:CO_2) is reduced from 70:30 to 30:70 [5].

An SOFC system can be divided into three main parts: (1) a fuel processor to reform the raw fuel into hydrogen gas, (2) SOFC stacks which subsequently generate electricity and useful heat from the reformed gas and (3) an afterburner where the residual fuel is combusted in order to supply heat to the preheaters and the fuel processor. Within the fuel processor, four main chemical reactions, namely steam reforming, dry

* Corresponding author. Tel.: +66 2 218 6868; fax: +66 2 218 6877.
E-mail address: Suttichai.A@chula.ac.th (S. Assabumrungrat).

1385-8947/$ – see front matter © 2007 Elsevier B.V. All rights reserved.
doi:10.1016/j.cej.2007.10.007

Nomenclature

$D_{A–B}$	ordinary diffusivity of gas A versus gas B [$cm^2\ s^{-1}$]
$D_{A–B(eff)}$	ordinary diffusivity of gas A versus gas B [$cm^2\ s^{-1}$]
$D_{A,k}$	Knudsen diffusivity of gas A [$cm^2\ s^{-1}$]
$D_{A,k(eff)}$	effective Knudsen diffusivity of gas A [$cm^2\ s^{-1}$]
$D_{i(eff)}$	effective diffusion coefficient of species i (i = anode, cathode) [$cm^2\ s^{-1}$]
D_p	catalyst pore diameter [μm]
E	open circuit voltage [V]
$E_{act,a}$	activation energy at anode [$J\ mol^{-1}$]
$E_{act,c}$	activation energy at cathode [$J\ mol^{-1}$]
F	Faraday constant (9.6495×10^4) [$C\ mol^{-1}$]
ΔG_i	Gibb's free energy of reaction i [$J\ mol^{-1}$]
i	current density [$A\ cm^{-2}$]
$i_{0,i}$	exchange current density (i = anode, cathode) [$A\ cm^{-2}$]
$K_{eq,dry}$	equilibrium constant of dry reforming reaction [Pa^2]
$K_{eq,pox}$	equilibrium constant of partial oxidation reaction [$Pa^{3/2}$]
$K_{eq,RWGS}$	equilibrium constant of reverse water gas shift reaction (RWGS)
$K_{eq,steam}$	equilibrium constant of steam reforming reaction [Pa^2]
l_a	thickness of anode [μm]
l_c	thickness of cathode [μm]
L	thickness of electrolyte [μm]
M_A	molecular weight of gas A [g]
n	electrode porosity
p_i^I	inlet pressure of species i [Pa]
P	operating pressure [Pa]
P_i	partial pressure of species i [Pa]
r	average radius of the catalyst pore [μm]
R	gas constant (8.3145) [$J\ mol^{-1}\ K^{-1}$]
T	operating temperature [K]
V	cell voltage [V]

Greek letter

α_c	carbon activity
ε_{AB}	Lennard-Jones energy interaction parameter scaled with respect to the Boltzman constant
γ_a	pre-exponential factor for anode exchange current density [$A\ m^{-2}$]
γ_c	pre-exponential factor for cathode exchange current density [$A\ m^{-2}$]
$\eta_{act,a}$	activation overpotential at anode [V]
$\eta_{act,c}$	activation overpotential at cathode [V]
$\eta_{Conc,a}$	concentration overpotential at anode [V]
$\eta_{Conc,c}$	concentration overpotential at cathode [V]
η_{ohmic}	ohmic overpotential [V]
σ_{AB}	collision diameter [Å]
Ω_D	collision integral
ξ	electrode tortuosity

reforming, partial oxidation and autothermal reforming are possible [6]. Dry reforming is perhaps the most interesting option for the conversion of biogas since the major constituents of the biogas are carbon dioxide and methane. However, it gives less hydrogen yields compared with steam reforming reaction. For steam and dry reforming, an external heat source is required to supply the endothermic fuel processor and to preheat the reforming agent (steam and CO_2) and this reduces the overall efficiency of the fuel processor. This problem can be overcome by applying an exothermic partial oxidation reaction which utilizes air as the reforming agent. However, it is accompanied by a lower hydrogen yield. Moreover, the hydrogen partial pressure of the gas product obtained from the partial oxidation is low due to the dilution effect of nitrogen present in air. In order to circumvent this drawback, the partial oxidation can operate simultaneously with steam reforming to improve hydrogen yield in a route referred to as autothermal reforming. If methane is the fuel, autothermal reforming leads to a higher efficiency (93.9%) – defined as the lower heating value (LHV) of hydrogen generated divided by the LHV of the methane fuel – than that of the steam reforming (91.3%) even though the latter gives a higher hydrogen yield. This is because higher heating power is required to generate steam in the case of the steam reforming. In addition, steam reforming is more prone to carbon formation compared to the partial oxidation and autothermal reforming [7].

When biogas is considered as a feedstock for the reformer, dry reforming may become a co-reaction due to the large amount of CO_2 present in biogas. However, the quantity of carbon dioxide available is not sufficient to convert all methane in biogas into hydrogen. Air and steam are the common reforming agents to combine with CO_2 in the fuel processor. The combination of the dry reforming with partial oxidation helps reduce the reformer size and softens the operating conditions. Furthermore, the desired H_2/CO ratio can be achieved by tuning the composition of the reforming agent [8–10]. Combined steam and dry reforming gives a higher H_2:CO ratio compared to sole dry reforming, however, large amount of heat must be supplied to the fuel processor [11,12].

Although the advantages and disadvantages of the use of each reforming agent in the fuel processor have been widely reported [11,12], the determination of a suitable reforming agent when the fuel processor is integrated with an SOFC system is still a matter for further investigation. The performance analysis of integrated biogas-fed SOFC systems should provide better insights into proper selection guidelines and hence, the rationale for this study. Thermodynamic analysis was performed to compare the relevant performance indices (overall electrical efficiency and the power density) of the SOFC systems with different reforming agents.

2. Modeling

2.1. Fuel processors

The main reaction in the fuel processor fed by biogas is the dry reforming reaction (Eq. (1)) due to the high content of carbon dioxide in biogas. When this is supplemented with steam, Eq.

(2) also takes place in the fuel processor. In a third option, air is fed along with biogas to the system so that the exothermic partial oxidation (Eq. (3)) occurs and provides the energy for the endothermic dry reforming.

$$CH_4 + CO_2 \rightarrow 2H_2 + 2CO \quad \text{(Dry reforming)} \tag{1}$$

$$CH_4 + H_2O \rightarrow 3H_2 + CO \quad \text{(Steam reforming)} \tag{2}$$

$$CH_4 + \tfrac{1}{2}O_2 \rightarrow 2H_2 + CO \quad \text{(Partial oxidation)} \tag{3}$$

It should be noted that the mildly endothermic reverse water gas shift reaction (RWGS) (Eq. (4)) always takes place in the fuel processor due to the present of CO_2 in biogas feed. This reaction inhibits the generation of hydrogen.

$$CO_2 + H_2 \rightarrow H_2O + CO \quad \text{(RWGS)} \tag{4}$$

The thermodynamics of dry and steam reforming are similar (since both are highly endothermic) while the methane partial oxidation is exothermic. However, carbon formation during dry reforming is more severe compared with that of steam reforming due to its lower H/C ratio [13]. In order to simplify the calculations, in this study the reformer is assumed to operate at isothermal condition and the exit gas reaches its equilibrium composition. The relationships of the thermodynamic equilibrium for the dry reforming, steam reforming, partial oxidation and RWGS are shown in Eqs. (5)–(8), respectively.

$$K_{\text{eq,dry}} = \frac{P_{H_2}^2 P_{CO}^2}{P_{CH_4} P_{CO_2}} \tag{5}$$

$$K_{\text{eq,steam}} = \frac{P_{H_2}^3 P_{CO}}{P_{CH_4} P_{H_2O}} \tag{6}$$

$$K_{\text{eq,pox}} = \frac{P_{H_2}^2 P_{CO}}{P_{CH_4} P_{O_2}^{1/2}} \tag{7}$$

$$K_{\text{eq,RWGS}} \rightleftarrows = \rightleftarrows \frac{P_{H_2O} P_{CO}}{P_{H_2} P_{CO_2}} \tag{8}$$

where $K_{\text{eq},i}$, the equilibrium constant of reaction i, can be calculated from this expression:

$$K_{\text{eq},i} = e^{-\Delta G_i / RT} \tag{9}$$

The possibility of carbon formation may be examined from the estimation of the carbon activity (α_c). The carbon formation is thermodynamically possible when $\alpha_c \geq 1$. The details of carbon activity calculations are described in our recent work [14]. In this study, the following carbon formation reactions are assumed to occur in the reformer.

$$2CO = CO_2 + C \tag{10}$$

$$CH_4 = 2H_2 + C \tag{11}$$

$$CO + H_2 = H_2O + C \tag{12}$$

where the carbon activities (α_c) for these carbon formation reactions can be calculated by Eqs. (13)–(15):

$$\alpha_{c,CO} = \frac{K_1 P_{CO}^2}{P_{CO_2}} \tag{13}$$

$$\alpha_{c,CH_4} = \frac{K_2 P_{CH_4}}{P_{H_2}^2} \tag{14}$$

$$\alpha_{c,CO\text{–}H_2} = \frac{K_3 P_{CO} P_{H_2}}{P_{H_2O}} \tag{15}$$

2.2. SOFC stack model

Electrochemical reaction takes place via the reaction between fuel and oxidizing agent. At the cathode section, oxygen in air is reduced to oxygen ions (Eq. (16)) which permeate via the solid electrolyte to react with the hydrogen fuel at the anode section (Eq. (17)). Only hydrogen is assumed to react electrochemically with oxygen ions. It was observed that the H_2 electro-oxidation is much faster than the CO electro-oxidation [15] and in addition the rate of WGS reaction is fast at high temperatures [16–18]. It is also assumed that little amount of methane remaining from the fuel processor is consumed via the steam reforming and that the anode compositions always reach their equilibrium along the cell length due to the fast kinetics at high temperature. For the SOFC stack, Ni-YSZ, YSZ and LSM-YSZ are used as the materials in the anode, electrolyte and cathode, respectively.

$$\tfrac{1}{2}O_2 + 2e^- \rightarrow O^{2-} \tag{16}$$

$$H_2 + 2O^{2-} \rightarrow H_2O + 2e^- \tag{17}$$

The open circuit voltage (E) of the cell can be calculated from the Nernst equation which is expressed as:

$$E = E^0 + \frac{RT}{2F} \ln\left(\frac{P_{H_2} P_{O_2}^{1/2}}{P_{H_2O}}\right) \tag{18}$$

The actual cell potential (V) is always less than the open circuit voltage (E) owing to the existence of overpotentials as shown in Eq. (19). The overpotentials can be categorized into three main sources: ohmic overpotential (η_{ohmic}), activation overpotential (η_{act}) and concentration overpotential (η_{Conc}).

$$V = E - \eta_{\text{act}} - \eta_{\text{ohmic}} - \eta_{\text{Conc}} \tag{19}$$

2.2.1. Ohmic overpotential (η_{ohmic})

This overpotential is the resistance to flow of electron through the electrodes and the interconnections as well as resistance to the flow of ions through electrolyte. This voltage drop is the vital one in all types of cells and is linearly proportional to current density (i). Due to the higher electronic conductivity of the electrodes compared to the electrolyte, only ohmic overpotential in the electrolyte is concerned. Hence, the ohmic overpotential of SOFC can be expressed by [19]:

$$\eta_{\text{ohmic}} = 2.99 \times 10^{-11} iL \exp\left(\frac{10300}{T}\right) \tag{20}$$

2.2.2. Activation overpotential (η_{act})

Activation overpotential is controlled by the kinetics at the electrode surface. It is directly related to the activation barrier to be overcome by the reacting species in order to conduct the electrochemical reaction. The electrode reaction rate at high temperatures is fast, leading to low activation polarization as normally observed in SOFC.

These activation overpotentials in electrodes can be expressed by the Butler-Volmer equation,

$$i = i_0 \left[\exp\left(\frac{\alpha z F \eta_{act}}{RT} \right) - \exp\left(-\frac{(1-\alpha) z F \eta_{act}}{RT} \right) \right] \quad (21)$$

In case of SOFC, α and z are set to 0.5 and 2 [20]. Therefore, the activation potential at the anode and cathode can be explicitly written as:

$$\eta_{act,j} = \frac{RT}{F} \sinh^{-1}\left(\frac{i}{2i_0} \right), \quad j = a, c \quad (22)$$

The exchange current density (i_0) for the cathode side depends on partial pressure of both hydrogen and water as well as the operating temperature [21,22]. For the anode side, i_0 depends on oxygen partial pressure and operating temperature as expressed in Eqs. (23)–(24) [23].

$$i_{0,a} = \gamma_a \left(\frac{P_{H_2}}{P_{ref}} \right) \left(\frac{P_{H_2O}}{P_{ref}} \right) \exp\left(-\frac{E_{act,a}}{RT} \right) \quad (23)$$

$$i_{0,c} = \gamma_c \left(\frac{P_{O_2}}{P_{ref}} \right)^{0.25} \exp\left(-\frac{E_{act,c}}{RT} \right) \quad (24)$$

2.2.3. Concentration overpotential (η_{Conc})

The concentration overpotential is the electrical loss owing to the difference between the reactant concentration on the reaction site and that in the bulk of the gas stream. This is due to the effect of the diffusion of the reactant gas into the pore of the electrochemical catalyst. It can be calculated by Eqs. (25) and (26):

$$\eta_{Conc,a} = \frac{RT}{2F} \ln\left[\frac{(1 + (RT/2F)(l_a / D_{a(eff)} p^I_{H_2O}) i)}{(1 - (RT/2F)(l_a / D_{a(eff)} p^I_{H_2}) i)} \right] \quad (25)$$

$$\eta_{Conc,c} = \frac{RT}{4F} \ln\left[\frac{p^I_{O_2}}{(p_c - \delta_{O_2}) - ((p_c - \delta_{O_2}) - p^I_{O_2}) \exp\left[(RT/4F)(\delta_{O_2} l_c / D_{c(eff)} p_c) i \right]} \right] \quad (26)$$

where δ_{O_2}, $D_{a(eff)}$ and $D_{c(eff)}$ can be expressed by:

$$\delta_{O_2} = \frac{D_{O_2,k(eff)}}{D_{O_2,k(eff)} + D_{O_2-N_2(eff)}} \quad (27)$$

$$\frac{1}{D_{c(eff)}} = \frac{\xi}{n} \left(\frac{1}{D_{O_2,k}} + \frac{1}{D_{O_2-N_2}} \right) \quad (28)$$

$$D_{a(eff)} = \left(\frac{p_{H_2O}}{p_a} \right) D_{H_2(eff)} + \left(\frac{p_{H_2}}{p_a} \right) D_{H_2O(eff)} \quad (29)$$

$$\frac{1}{D_{H_2(eff)}} = \frac{\xi}{n} \left(\frac{1}{D_{H_2,k}} + \frac{1}{D_{H_2-H_2O}} \right) \quad (30)$$

$$\frac{1}{D_{H_2O(eff)}} = \frac{\xi}{n} \left(\frac{1}{D_{H_2O,k}} + \frac{1}{D_{H_2-H_2O}} \right) \quad (31)$$

The correlation between the effective parameter and the normal parameter can be expressed by Eq. (32)

$$D_{(eff)} = \frac{n}{\xi} D \quad (32)$$

Knudsen diffusivity can be computed by the correlation below:

$$D_{A,k} = 9700 r \sqrt{\frac{T}{M_A}} \quad (33)$$

Ordinary diffusivity can be calculated by Chapman-Enskog equation (Eq. (34)) [24]:

$$D_{A-B} = 1.8583 \times 10^{-3} \left(\frac{T^{3/2}((1/M_A)+(1/M_B))^{1/2}}{P \sigma^2_{AB} \Omega_D} \right) \quad (34)$$

where σ_{AB} is the collision diameter (Å) which is equal to $(\sigma_A + \sigma_B)/2$. Ω_D is computed from [25]:

$$\Omega_D = \frac{A}{T_k^B} + \frac{C}{\exp(DT_k)} + \frac{E}{\exp(FT_k)} + \frac{G}{\exp(HT_k)} \quad (35)$$

where T_k is equal to T/ε_{AB} and A, C, E and G are constants for each gas.

2.3. Afterburner and heat exchanger

At the exit of the SOFC stack, the anode exit gas and the cathode exit gas are mixed for post combustion. Complete combustion is assumed to take place in the afterburner; hence methane, carbon monoxide and hydrogen contents in the exhaust gas become zero. The heat exchanger is assumed to operate without heat loss.

2.4. Calculation procedure for determining SOFC stack performance

For the SOFC operation, a constant operating voltage along the cell length is assumed as the current collector usually has high electrical conductivity. The operating voltage is kept at 0.7 V in this study. The current density inside the stack varies with the distance from the stack entrance due to the changes in gas compositions in the cathode and anode sections and therefore the open circuit voltage. Hence, the average current density and power density of the SOFC stack can be calculated. In this work, the calculation takes place for each small fuel utilization region employing the mathematical model presented in Section 2.2. The thermodynamic equilibrium is assumed for the anode gas in each region because the anode material is also active for the reactions and the operating temperature of the SOFC stack is high. In each region, the open circuit voltage, overpotentials,

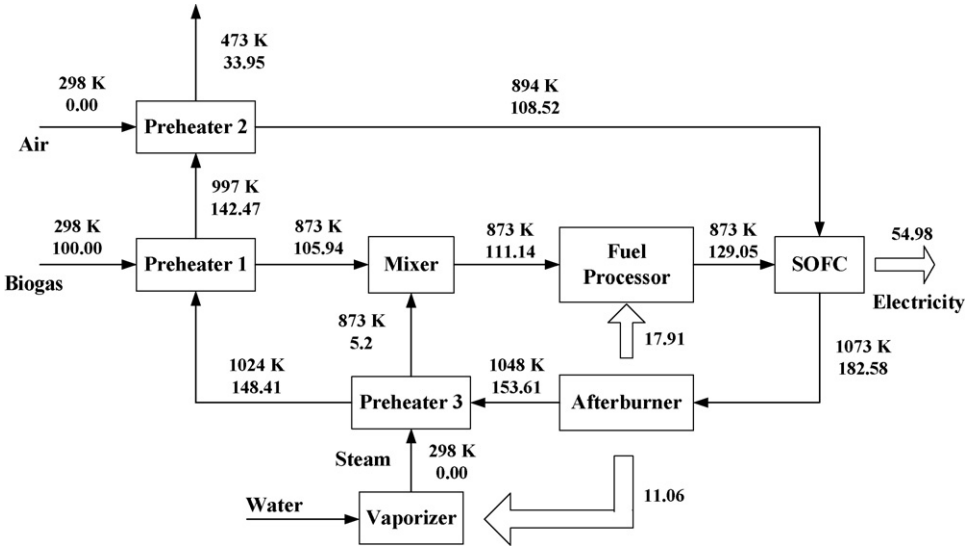

Fig. 1. The plant configuration and energy balance for the steam-fed SOFC system.

equilibrium composition of anode fuel, stack area and current density are computed. The stack areas calculated in each region are added up to yield the total stack area. Finally, the current calculated from the fuel utilized in the stack is divided by the total stack area to obtain the average current density and hence, the average power density is determined. The electrical efficiency may be computed from Eq. (36).

$$\text{SOFC plant efficiency} = \frac{\text{total electricity generated}}{\text{LHV of biogas feed}} \tag{36}$$

2.5. SOFC system configurations

Three biogas-fuelled SOFC systems are considered in this study, i.e. SOFC using steam as the reforming agent (steam-fed SOFC), SOFC using air as the reforming agent (air-fed SOFC) and SOFC using both air and steam as the reforming agents (co-fed SOFC). The plant configuration for the steam-fed SOFC is illustrated in Fig. 1. Several unit operations are included in this configuration consisting of a fuel processor, SOFC stack, an afterburner, a mixer, a vaporizer and preheaters. Steam is generated via the vaporizer, preheated and then mixed with biogas. The mixture gas is then fed into the fuel processor. In the fuel processor, the steam reforming, dry reforming and WGS take place to produce H_2-rich gas and the total heat consumed in these reactions is supplied from heat generated in the afterburner. The H_2-rich gas produced in the fuel processor is fed into the SOFC stack where the electrical energy is generated. The heat generated in the SOFC stack due to the irreversibility is utilized for air and H_2-rich gas preheating. The residue fuel gas released from the SOFC stack is burned up in the afterburner in order to supply heat to the vaporizer and the fuel processor. A high temperature flue gas which mainly contains carbon dioxide and steam released from the afterburner is used in preheating

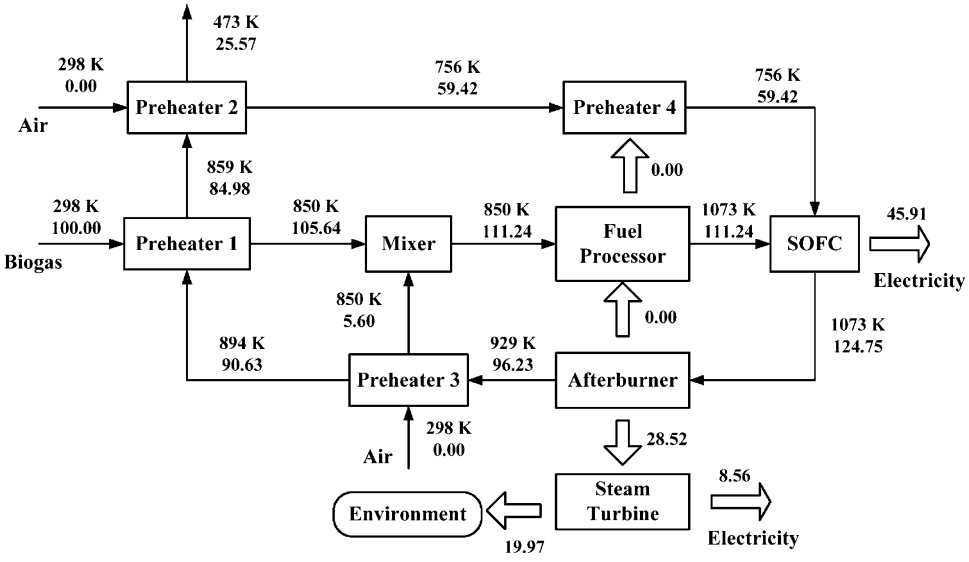

Fig. 2. The plant configuration and energy balance for the air-fed SOFC system.

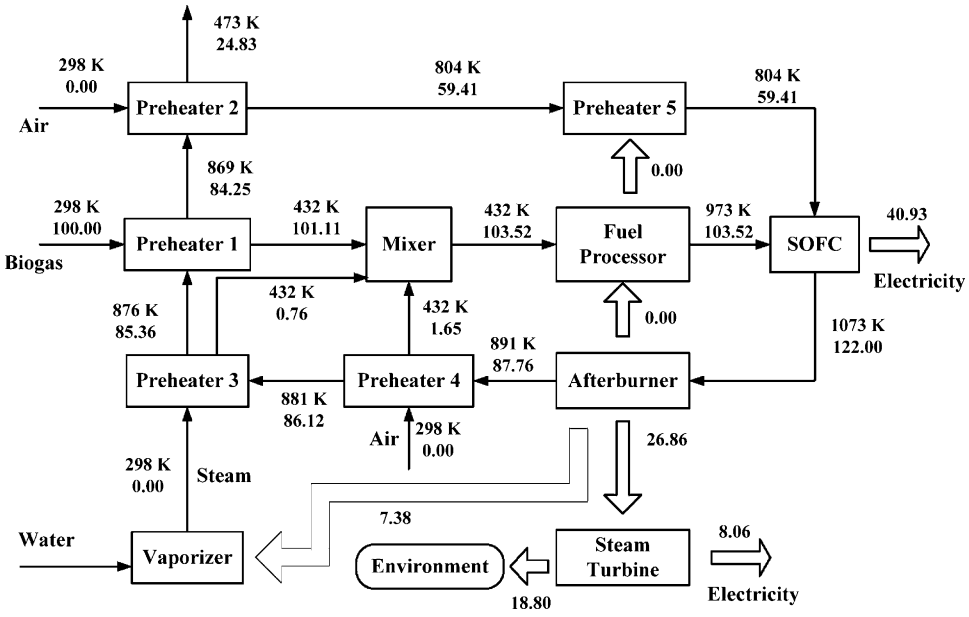

Fig. 3. The plant configuration and energy balance for the co-fed SOFC system.

biogas, steam and oxidizing agent (air) before being discharged to the environment at low temperature. For the calculation, the flue gas temperature released from the system is kept at 473 K. The total heating power used in preheating is computed and the afterburner outlet gas temperature and the quantity of the fuel combusted in the afterburner to achieve the required outlet gas temperature are then calculated. To achieve a desired temperature of the SOFC stack, an oxidizing agent (air) temperature is tuned up employing the energy balance in the SOFC stack. A trial-and-error is performed by tuning the fuel utilization until the total energy flowing into the afterburner is equal to the total energy flowing out of the afterburner. For the air-fed SOFC, its calculation procedure is similar to that of the steam-fed SOFC. However, the heating power used in preheating and the quantity of the fuel used in the afterburner of the former is extremely less than the latter. Therefore, almost all hydrogen in the anode gas can be utilized in the SOFC stack for the air-fed SOFC and the power density also reduces following to the increase in the fuel utilization. To achieve a reasonable power density, the hydrogen mole fraction of the SOFC anode output stream is controlled to be higher than 1.5 mol%. In this case, the heat residue from the afterburner is fed into the steam turbine to generate more electricity as illustrated in Fig. 2. The electrical efficiency of steam turbine is assumed to be 30%. The heat generated from the exothermic partial oxidation in the fuel processor is utilized in preheating the oxidizing agent.

According to the plant configuration of the co-fed SOFC, most of the configurations are identical to that of the air-fed SOFC as illustrated in Fig. 3; nevertheless, more heat is generated in the afterburner in order to generate steam. It should be noted that, in all cases, the quantities of air fed as the oxidant into the SOFC cathode are 5 times of theoretical air required to combust the biogas fuel. The excessive amount of air is required in order to avoid the overheating of the stack which would cause cell damages.

3. Results and discussion

The models of the SOFC systems are programmed in Visual Basic. The values of all parameters used in the calculations are summarized in Table 1. For model validation, the computed results are compared with the experimental results of Zhao and Virkar [26] and Tao et al. [27]. The feed compositions and the SOFC stack dimensions used in model validation are summarized in Table 2. As shown in Fig. 4, the simulation shows good agreement with the experimental data using pure hydrogen fuel [26] for all temperature levels particularly at the operating temperature of 1073 K which is used in the subsequent studies of this work. Moreover, with inlet gas containing various fuel types (CH_4–CO–H_2), the simulation could also predict the experimental data [27] well as illustrated in Fig. 5.

Table 1
Summary of model parameters [28]

Parameters	Value
γ_a	1.344×10^{10} A m^{-2}
γ_c	2.051×10^{9} A m^{-2}
$E_{act,a}$	1.0×10^{5} J mol^{-1}
$E_{act,c}$	1.2×10^{5} J mol^{-1}
n	0.48
ξ	5.4
D_p	1 μm
d_a	750 μm
d_c	50 μm
L	50 μm
V	0.7 V
T_{SOFC}	1073 K
Operating pressure (SOFC)	1 bar
Operating pressure (H_2 processor)	1 bar
$T_{Fuel\ processor\ (steam\ as\ reforming\ agent)}$	873 K
$T_{Fuel\ processor\ (air\ as\ reforming\ agent)}$	1073 K

Table 2
Feed compositions and SOFC stack dimensions used in model validation

Parameters	Zhao and Virkar [26]	Tao et al. [27]
Fuel compositions (mole fraction)		
CH_4	–	0.21
H_2	0.97	0.4
CO	–	0.2
CO_2	–	0.18
N_2	–	0.01
H_2O	0.03	–
Stack dimensions		
Type of cell	Button cell	Planar SOFC with 100 cm^2 active surface area
n	0.48	0.48
ξ	5.4	5.4
D_p	1 μm	1 μm
d_a	1000 μm	500 μm
d_c	20 μm	50 μm
L	8 μm	10 μm
Stack average temperature	873–1073 K	1073 K

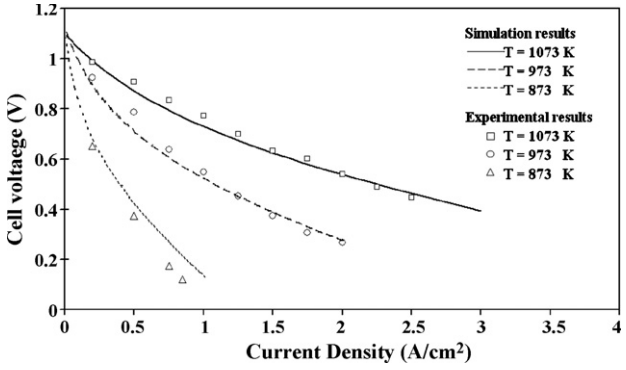

Fig. 4. Verification of the SOFC model.

The boundaries of carbon formation indicating the minimum amount of a reforming agent required to avoid the carbon formation for the biogas steam reforming and partial oxidation are illustrated in Fig. 6a and b, respectively. It is obvious that less reforming agent (steam or air) is required in order to inhibit the carbon formation when the reforming temperature increases. In fact, the moles of reforming agent per biogas required decreased almost hyperbolically with temperature attaining nearly constant value beyond about 1173 K. Biogas with a higher content of methane is more prone to carbon formation than that with a lower amount of methane. These trends are corresponding well with previous literatures [13,14,29]. Note that in the following studies the SOFC systems are always operated using a sufficient amount of the reforming agent to avoid the carbon formation.

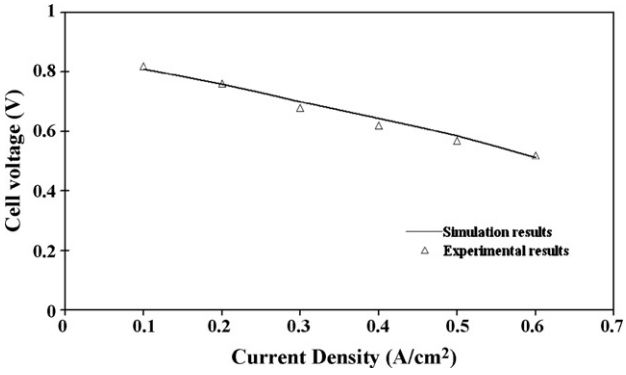

Fig. 5. Verification of SOFC model for the feed with CH_4, CO and H_2 mixtures.

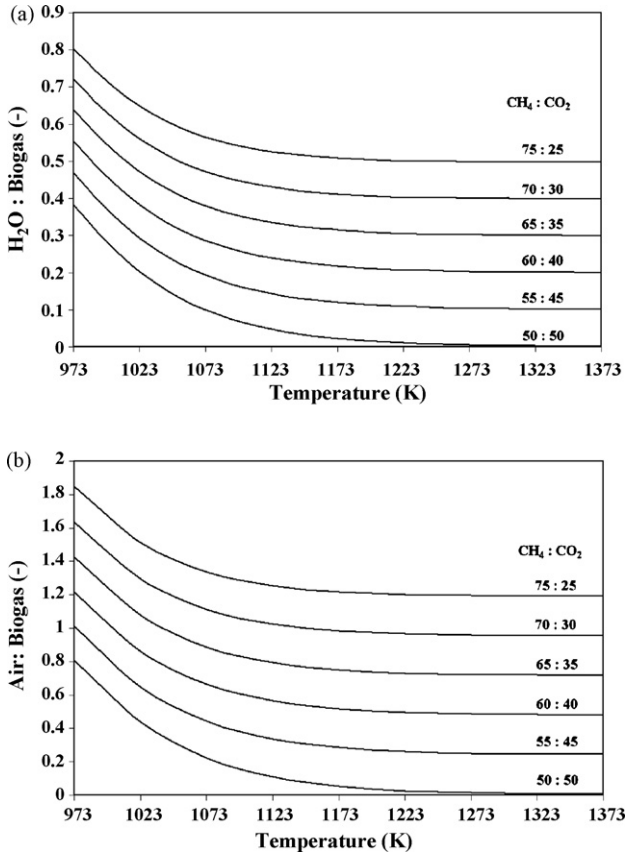

Fig. 6. Boundary of carbon formation for the biogas-fed fuel processors with different reforming agents: (a) steam and (b) air.

The electrical efficiency and power density of the steam-fed SOFC were first investigated. Energy value (lower number on each stream) and temperature (upper number) for different sections of the plant are shown in Fig. 1. The values of H_2O:biogas, CH_4:CO_2 in biogas and fuel processing temperature are 1.2, 60:40 and 873 K, respectively. It may be noted that the energy is given as a percentage of lower heating value of the biogas fuel. As seen in Fig. 1, large amounts of heat generated in afterburner, about 11.06 and 17.91% of biogas LHV, respectively, are supplied to the vaporizer and the fuel processor. An overall electrical efficiency of about 55% of biogas LHV was obtained for this SOFC system. Fig. 7 shows the plant electrical efficiency and power density of the steam-fed SOFC at various steam contents and CH_4:CO_2 ratios. As shown in Fig. 7, biogas with a higher CH_4:CO_2 ratio gives higher efficiency than that with a lower one. As the methane content in the biogas increases, the reformed gas contains hydrogen at a higher concentration and, therefore, a higher power density is achieved. The smaller content of CO_2 in the biogas reduces the energy loss by the exhaust gas of the system. Consequently, the electrical efficiency is improved. Inter-

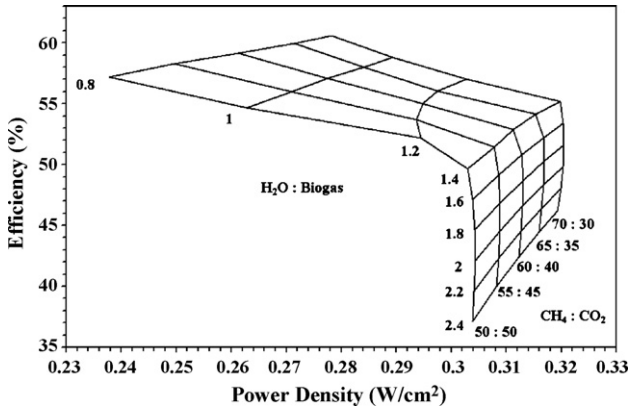

Fig. 7. Performance of the steam-fed SOFC at different H_2O:biogas and CH_4:CO_2 ratios (fuel processing temperature = 873 K).

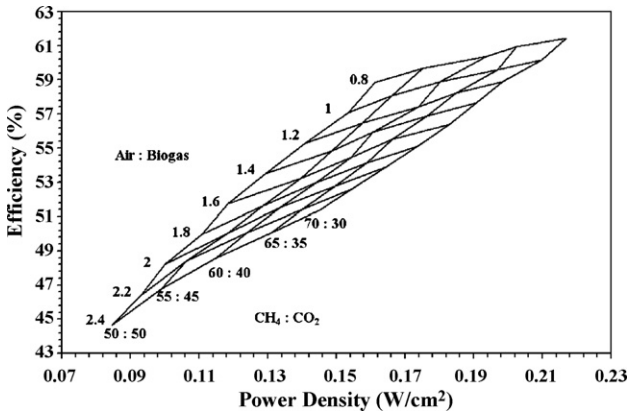

Fig. 8. Performance and current density of air-fed SOFC at different air:biogas and CH_4:CO_2 ratios in biogas (fuel processing temperature = 1073 K).

estingly, as the H_2O:biogas ratio increases, the plant electrical efficiency decreases. This is particularly pronounced when the H_2O:biogas ratio is higher than 1.6. Although excessive addition of steam in the system can increase the hydrogen yield from the reformer, significant amount of heat load is required to generate and preheat the excessive steam. Consequently, the SOFC cannot be operated at high fuel utilization, resulting in lower electrical efficiency. It is also observed that the power density increases initially, levels off and then slightly decreases. This behavior is most likely due to the fact that although steam is essential for promoting the production of hydrogen, it also acts as a diluent, leading to the decrease of hydrogen concentration and power density.

In the case of the air-fed SOFC, the plant configuration and its energy balance are illustrated in Fig. 2, the values of air:biogas, CH_4:CO_2 in biogas and fuel processing temperature are 1.6, 60:40 and 1073 K, respectively. Unlike the steam-fed SOFC, heating energy is not required for the steam generator and the fuel processor. However, hydrogen fuel cannot be used entirely in the SOFC stack, as some fuel must remain in the SOFC outlet stream in order to maintain a high power density for the SOFC. The residue gas combusted as well as the energy generated (28.52% of biogas LHV) is utilized in the steam turbine (assuming an electrical efficiency of 30%) to generate more electricity as shown in Fig. 2. Heat loss generated in the steam turbine (19.97% of biogas LHV) is released to the environment. The plant efficiency and power density for the air-fed SOFC with various air:biogas and CH_4:CO_2 ratios are illustrated in Fig. 8. Compared with the case of the steam-fed SOFC, the power density is much lower. This is due to the fact that the partial oxidation reaction (Eq. (2)) can produce only 2 moles of hydrogen per mole of methane compared with 3 moles of hydrogen per mole of methane in the case of the steam reforming reaction (Eq. (3)). In addition, the high proportion of nitrogen present in air also reduces the hydrogen concentration in the reformed gas. Consequently, the hydrogen partial pressure of the product gas derived from the partial oxidation is lower than that derived from the steam reforming, leading to a lower SOFC power density. However, the air-fed SOFC offers slightly higher electrical efficiency than the steam-fed system. This is due to the exothermicity of the partial oxidation route. Therefore, heat energy from the afterburner is not required to supply to the fuel processor unlike the steam-fed SOFC. Moreover, energy is not required for steam generation which usually consumes large amount of heat. These features help to annul the effect of reduced hydrogen yield in the partial oxidation route. Similar to the case of the steam-fed SOFC, both plant efficiency and power density improve as the quantity of methane in biogas increases as illustrated in Fig. 8. The effect of variation in the air:biogas ratio was also investigated. The results indicate that both power density and overall efficiency decrease with increasing the air content. The decrease in power density is mainly due to the significant increase in inert nitrogen in the inlet stream (anode). The decrease in the electrical efficiency may be ascribed to the excessive air fed to the reformer, occasioning higher energy loss from the increased amount of exhaust gas.

As a third option, the co-fed SOFC is also investigated and its energy balance is illustrated in Fig. 3. The values of H_2O:biogas, air:biogas, CH_4:CO_2 in biogas and fuel processing temperature are 0.8, 2, 60:40 and 973 K, respectively. Unlike the steam-fed SOFC, there is no energy supplied to the fuel processor due to the participation of exothermic partial oxidation reaction; however, some heating energy produced in the afterburner (7.38% of biogas LHV) must be supplied to the vaporizer to generate steam. Furthermore, the residue heat from the co-fed SOFC system (26.86% of biogas LHV) is supplied to the steam turbine to generate more electricity like in the case of the air-fed SOFC. The heat loss from the gas turbine (18.8% of biogas LHV) is released to the environment. The plant electrical efficiency and the power density at different air:biogas and H_2O:biogas ratios are illustrated in Fig. 9. In this study, the biogas composition (CH_4:CO_2) is kept at 60:40. From the foregoing analysis, the electrical efficiency of the co-fed SOFC decreases with the increase in the reforming agent content. The power density decreases as the air:biogas ratio increases due to the presence of large amount of nitrogen in air. However, an optimum H_2O:biogas ratio which provides a maximum power density is observed. This is due to the competing effects between the promotion of hydrogen production and the dilution effect by the addition of more water.

In order to select a suitable reforming agent, the performance of the SOFC systems with different reforming agents is com-

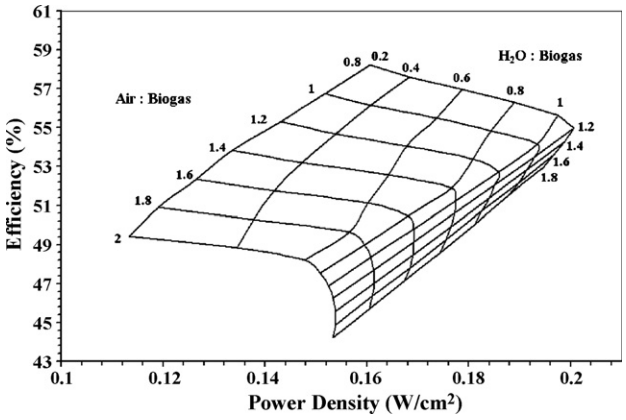

Fig. 9. Performance and current density of co-fed SOFC at different air:biogas and H_2O:biogas ratios (fuel processing temperature = 973 K).

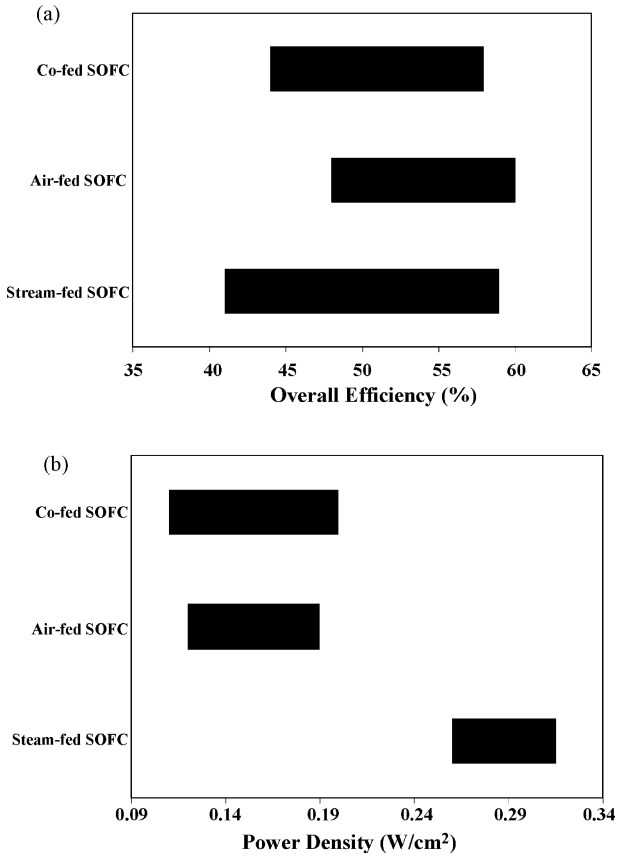

Fig. 10. SOFC performance: (a) overall electrical efficiency and (b) power density (CH_4:CO_2 = 60:40).

pared as shown in Fig. 10. It is obvious that steam is the most attractive reforming agent for the biogas-fed SOFC regarding the power density. Although the air-fed SOFC can provide slightly higher electrical efficiency than the steam-fed SOFC, the power density is much lower due to the high content of nitrogen in air. By adding steam to the air-fed SOFC, the power density can be improved but with the reduction of the electrical efficiency. Because the stack is among the most expensive part of the SOFC system, it is likely that the use of steam as the reforming agent is the most suitable for the biogas-fed SOFC although the electrical efficiency is slightly lower than the use of air.

In order to improve the efficiency of the steam-fed SOFC, the biogas split option is proposed as illustrated in Fig. 11. For this operation, part of biogas is split from the fuel processor and directly fed to the afterburner. This diminishes the heat load in the SOFC system due to the decrease in the quantities of steam added. Moreover, the extent of the endothermic steam reforming reaction is also diminished. As seen in Fig. 11, the heat load in steam generator and H_2 processor for the steam-fed SOFC with 9% of biogas split are 10.1 and 16.3% of biogas LHV, respectively, which are lower compared with those for the steam-fed SOFC without the biogas split (11.1 and 17.9% of biogas LHV for the heat load in steam generator and H_2 processor, respectively). The heating power and the heat exchanger area required in preheating are also reduced. Consequently, the electrical efficiency can be increased while the capital cost is also reduced. The results of the biogas split option shown in Fig. 12 indicate

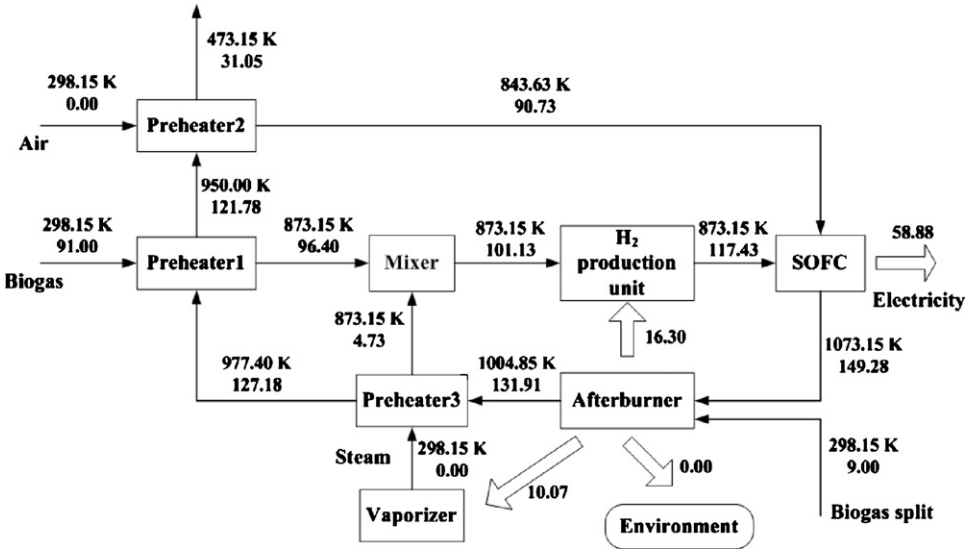

Fig. 11. The SOFC configuration with the biogas split operation.

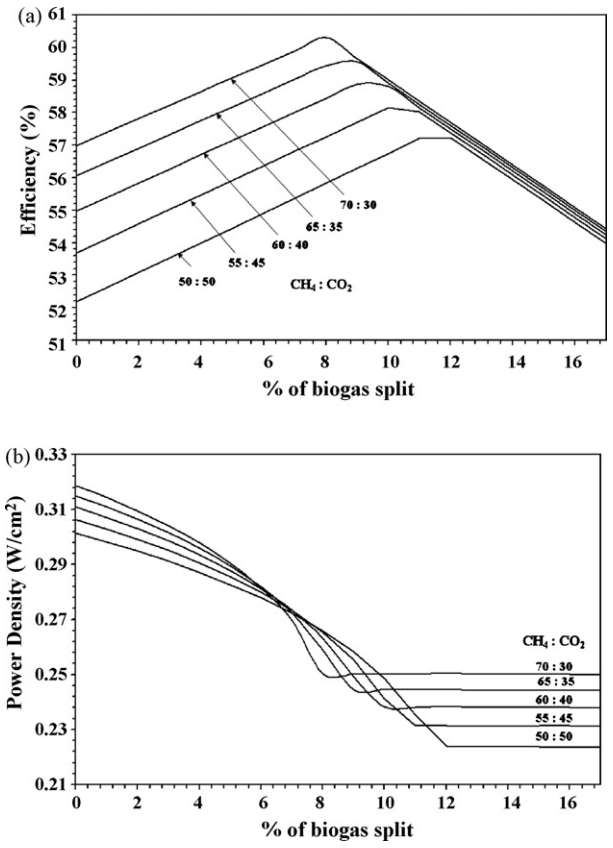

Fig. 12. The effect of %biogas split on (a) overall electrical efficiency and (b) power density at different biogas compositions (fuel processing temperature = 873 K, H_2O:biogas = 1.2).

that the increase in the percentage of biogas split can improve the plant efficiency. However, there is an optimal point at which the SOFC achieves a maximum electrical efficiency. For the operation over this point, the plant efficiency decreases with increasing the percentage of biogas split since the heat released from the afterburner is higher than that required in the vaporizer and the fuel processor. With the installation of biogas split operation, 59% of overall electrical efficiency can be achieved compared to 55% for the normal case with the CH_4:CO_2 ratio of 60:40. Although the biogas split can improve the plant electrical efficiency, the power density always decreases with the increasing biogas split, implying that more SOFC stack area is required for the higher percentage of biogas split. However, it should be noted that the use of steam-fed SOFC with biogas split still offers higher power density than the air-fed SOFC while the electrical efficiency becomes comparable.

4. Conclusions

Performance of the biogas-fed SOFC systems with different reforming agents (steam, air and combined steam/air) was determined in order to find a suitable reforming agent. The boundary of carbon formation was firstly calculated to specify a minimum amount of each reforming agent necessary to avoid carbon formation. Within the range of operating variables examined (chosen to avoid debilitating carbon formation), it seems that when the amount of reforming agent increases, the electrical efficiency always decreases. For the steam-fed SOFC, there is an optimal amount of steam which provides a maximum power density. However, for the air-fed SOFC, the power density always decreases with the increased amount of air due to the dilution effect of nitrogen in air. Steam is considered to be the most suitable reforming agent in this study as the steam-fed SOFC offers much higher power density than the air-fed SOFC although its electrical efficiency is slightly lower due to the high energy requirement in the steam generation. When steam is added in the air-fed SOFC as in the case of the co-fed SOFC, the power density can be improved but the electrical efficiency becomes lower compared with the case of the air-fed SOFC. In order to improve the electrical efficiency of the steam-fed SOFC, the biogas split option was considered. It was found that a higher electrical efficiency can be achieved. In addition, although the power density is lowered by this operation, the value is still higher than the case of the air-fed SOFC.

Acknowledgements

This research is financially supported by the Thailand Research Fund and Commission on Higher Education.

References

[1] J. Van Herle, Y. Membrez, O. Bucheli, Biogas as a fuel source for SOFC co-generators, J. Power Sources 127 (2004) 300–312.
[2] D.C. Dayton, Fuel cell integration—a study of the impacts of gas quality and impurities, NREL Final Report, 2001.
[3] J. Van herle, F. Maréchal, S. Leuenberger, Y. Membrez, O. Bucheli, D. Favrat, Process flow model of solid oxide fuel cell system supplied with sewage biogas, J. Power Sources 131 (2004) 127–141.
[4] R. Layi Fagbenle, A.B.C. Oguaka, O.T. Olakoyejo, A thermodynamic analysis of a biogas-fired integrated gasification steam injected gas turbine (BIG/STIG) plant, Appl. Therm. Eng. 27 (2005) 2220–2225.
[5] M. Jenne, T. Dörk, A. Schuler, in: U. Bossel (Ed.), Proceedings of the Fifth European Solid Oxide Fuel Cell Forum, Lucerne, Switzerland, July 2002, European Forum Secretariat, CH 5442 Oberrohrdorf, Switzerland, 2002, pp. 460–466.
[6] P. Ferreira-Aparicio, M.J. Benito, J.L. Sanz, New trends in reforming technologies: from hydrogen industrial plants to multifuel microreformers, Catal. Rev. 47 (2005) 491–588.
[7] S. Ahmed, M. Krumpelt, Hydrogen from hydrocarbon fuels for fuel cells, Int. J. Hydrogen Energy 26 (2001) 291–301.
[8] J.R. Rostrup-Nielsen, Syngas in perspective, Catal. Today 71 (2002) 243–247.
[9] P.D.F. Vernon, M.L.H. Green, A.K. Cheetham, A.T. Ashcroft, Partial oxidation of methane to synthesis gas, and carbon dioxide as an oxidising agent for methane conversion, Catal. Today 13 (1992) 417–426.
[10] A.M. O'Connor, J.R.H. Ross, The effect of O_2 addition on the carbon dioxide reforming of methane over Pt/ZrO_2 catalysts, Catal. Today 46 (1998) 203–210.
[11] G.F. Froment, Production of synthesis gas by steam- and CO_2-reforming of natural gas, J. Mol. Catal. A: Chem. 163 (2000) 147–156.
[12] J.R. Rostrup-Nielsen, J. Sehedsted, J.K. Norskov, Hydrogen and synthesis gas by steam- and CO_2 reforming, Adv. Catal. 47 (2002) 65–139.
[13] J.H. Edwards, A.M. Maitra, The chemistry of methane reforming with carbon dioxide and its current and potential applications, Fuel Proc. Technol. 42 (1995) 269–289.
[14] S. Assabumrungrat, N. Laosiripojana, P. Piroonlerkgul, Determination of the boundary of carbon formation for dry reforming of methane in a solid oxide fuel cell, J. Power Sources 159 (2006) 1274–1282.

[15] M.A. Khaleel, Z. Lin, P. Singh, W. Surdoval, A finite element analysis modeling tool for solid oxide fuel cell development: coupled electrochemistry, thermal and flow analysis in MARC, D. Collin, J. Power Sources 130 (2004) 136–148.
[16] M.C.J. Bradford, M.A. Vannice, Catalytic reforming of methane with carbon dioxide over nickel catalysts. II: Reaction kinetics, Appl. Catal. A: Gen. 142 (1996) 97–122.
[17] H.M. Swaan, V.C.H. Kroll, G.A. Martin, C. Mirodatos, Deactivation of supported nickel catalysts during the reforming of methane by carbon dioxide, Catal. Today 21 (1994) 571–578.
[18] R. Blom, I.M. Dahl, A. Slagtem, B. Sortland, A. Spjelkavik, E. Tangstad, Carbon dioxide reforming of methane over lanthanum-modified catalysts in a fluidized-bed reactor, Catal. Today 21 (1994) 535–543.
[19] J.R. Ferguson, J.M. Fiard, R. Herbin, Three-dimensional numerical simulation for various geometries of solid oxide fuel cells, J. Power Sources 58 (1996) 109–122.
[20] S.H. Chan, K.A. Khor, Z.T. Xia, A complete polarization model of a solid oxide fuel cell and its sensitivity to the change of cell component thickness, J. Power Sources 93 (2001) 130–140.
[21] S.P. Jiang, S.P.S. Badwal, H_2 Oxidation reactions at the Ni and Pt electrodes on Y-TZP electrolytes, J. Electrochem. Soc. 144 (1997) 3777–3784.
[22] S.P. Jiang, S.P.S. Badwal, An electrode kinetics study of H_2 oxidation on Ni/Y_2O_3–ZrO_2 cermet electrode of the solid oxide fuel cell, Solid State Ionics 123 (1999) 209–224.
[23] J. Fleig, Solid oxide fuel cell cathodes: polarization mechanisms and modeling of the electrochemical performance, Annu. Rev. Mater. Res. 33 (2003) 361–382.
[24] W.J. Massman, A review of the molecular diffusivities of H_2O, CO_2, CH_4, CO, O_3, SO_2, NH_3, N_2O, NO, and NO_2 in air, O_2 and N_2 near STP, Atmos. Environ. 32 (1998) 1111–1127.
[25] H. Yakabe, M. Hishinuma, M. Uratani, Y. Matsuzaki, I. Yasuda, Evaluation and modeling of performance of anode-supported solid oxide fuel cell, J. Power Sources 86 (2000) 423–431.
[26] F. Zhao, A.V. Virkar, Dependence of polarization in anode-supported solid oxide fuel cells on various cell parameters, J. Power Sources 141 (2005) 79–95.
[27] G. Tao, T. Armstrong, A. Virkar, Intermediate temperature solid oxide fuel cell (IT-SOFC) research and development activities at MSRI, in: Nineteenth Annual ACERC&ICES Conference, Utah, 2005.
[28] M. Ni, M.K.H. Leung, D.Y.C. Leung, Parametric study of solid oxide fuel cell performance, Energy Convers. Manage. 48 (2007) 1525–1535.
[29] S.H. Lee, W. Cho, W.S. Ju, B.H. Cho, Y.C. Lee, Y.S. Baek, Tri-reforming of CH_4 using CO_2 for production of synthesis gas to dimethyl ether, Catal. Today 87 (2003) 133–137.